Mon. Not. R. Astron. Soc. **279,** 511–520 (1996)

Physical conditions in the transition regions around the Ring Nebula and NGC 7027

X.-W. Liu and M. J. Barlow

Department of Physics and Astronomy, University College London, Gower Street, London WC1E 6BT

Accepted 1995 October 9. Received 1995 October 9; in original form 1995 August 18

ABSTRACT

Deep long-slit spectra have been obtained in order to map the electron temperature and density in the warm transition regions around the Ring Nebula using the optical [C I] and [N I] forbidden lines. For the first time the [C I] λ8727 line is detected and mapped in this nebula. The temperature-sensitive [C I] nebular to auroral line ratio $(\lambda 9824 + \lambda 9850)/\lambda 8727$ yields a mean electron temperature of 8250 K, while variations of up to 2000 K can be seen for emission from the different parts of the nebula. The electron density derived from the density-sensitive [N I] doublet ratio, $\lambda 5198/\lambda 5200$, is similar to that deduced for the fully ionized regions using the [Cl III] $\lambda 5517/\lambda 5537$ doublet ratio. As compared with lines from ionized regions, the [C I] and [N I] lines show dramatic and complex variations, both in their surface brightness distributions and in their radial velocities along the nebular minor axis, in a manner largely consistent with the bipolar model proposed by Bryce, Balick & Meaburn for the Ring Nebula. The bulk material movement revealed by the large outflow velocities in the transition regions (up to ± 35 km s^{-1}), relative to the ionized regions, is likely to generate strong shocks, and thus provides a natural excitation mechanism for the strong near-infrared H_2 emission lines observed in the Ring Nebula. We have also observed NGC 7027. The new observations confirm the earlier results of Danziger & Goad, who found a very small $(\lambda 9824 + \lambda 9850)/\lambda 8727$ ratio for NGC 7027 and correctly attributed it as due to collisional de-excitation of the upper levels of the [C I] nebular lines under the very high-density conditions found in NGC 7027.

Key words: atomic processes – planetary nebulae: general – planetary nebulae: individual: NGC 6720 – planetary nebulae: individual: NGC 7027.

1 INTRODUCTION

The spatial distribution of near-infrared H_2 emission observed in old extended planetary nebulae (PNe) such as the Ring Nebula (M57, NGC 6720), NGC 3132 and 6853 (Storey 1984; Greenhouse, Hayward & Thronson 1988; Reay, Walton & Atherton 1988; Zuckerman & Gatley 1988; Kastner et al. 1994) is found to largely follow that of the [O I] λ6300 line, suggesting that the emitting molecules lie close to the transition regions. Recent detections of HCO^+ and HCN in NGC 6072 and IC 4406 indicate on-going chemistry which is likely to be dominated by photodissociation, shocks and ion–molecule reactions (Cox et al. 1992). Thus, the physical conditions, such as the temperature, particle density and radiation field density, prevailing in the partially ionized transition regions, which serve as boundary conditions for the neutral components, may prove to play a vital role in the interpretation of the origin, excitation and chemistry of the neutral components in these objects.

In the optical, the warm transition regions are usually studied using the [O I] $\lambda\lambda$5577, 6300 and 6363 lines (e.g. Richer, McCall & Martin 1991). The $(\lambda 6300 + \lambda 6363)/\lambda 5577$ ratio is a sensitive temperature diagnostic and thus can be used to derive temperatures in these regions. However, the terrestrial atmosphere is also a strong [O I] line emitter, and the relatively weak λ5577 line can be easily lost in the overwhelming atmospheric line. Recently, Liu et al. (1995a, Paper I) used the [C I] $\lambda\lambda$8727, 9824 and 9850 lines to measure the electron temperature and density in the transition regions around four PNe, all previously known to show strong molecular H_2 emission. In that paper, we showed that, unlike their counterpart from

photodissociation regions (PDRs; Münch & Hippelein 1982) around H II regions, where the line emissivities are dominated by radiative recombinations of C^+ ions with electrons (Escalante, Sternberg & Dalgarno 1991), the [C I] lines from these PNe were collisionally excited by electron impacts. As a result, the measured ratio $\Re_1 \equiv (\lambda 9824 + \lambda 9850)/\lambda 8727$, which is sensitive to temperature in the case of collisional excitation, provides a direct measure of the temperature in the warm transition regions around the PNe. Liu et al. found that the values of T_e derived from $\Re_1$ were smaller by about 2000 K than those deduced for the same object for higher excitation lines, such as [O III], [N II] and [S III], emitted in the ionized regions. We also found that the electron densities deduced from the density-sensitive [N I] line ratio $\Re_2 \equiv \lambda 5198/\lambda 5200$, did not show significant differences from the values deduced for the ionized regions.

Here we extend our observations of the [C I] and [N I] lines to the Ring Nebula and NGC 7027. The [C I] lines were first identified and measured in NGC 7027 by Danziger & Goad (1973). Their low-resolution sequential scanner observations, however, did not resolve the $\lambda 8727$ line from the nearby Pa 12 line at 8750 Å. Jewitt et al. (1983) mapped the [C I] nebular lines $\lambda\lambda 9824$, 9850 along five long slits parallel to the major axis of the Ring Nebula. However, they failed to detect the weaker [C I] auroral line $\lambda 8727$. Thus, the [C I] temperature in the Ring Nebula remains to be measured. The deep long-slit spectra obtained here allow us not only to detect the $\lambda 8727$ line for the first time in this nebula but also to map the [C I] temperature and [N I] electron density across the nebular surface. Although the spectral resolution used here was not sufficient to resolve the nebular expansion, the data reveal remarkable [C I] and [N I] radial velocity variations along the minor axis of the Ring Nebula.

2 OBSERVATIONS AND DATA REDUCTION

The data were obtained at the 4.2-m William Herschel Telescope (WHT) at La Palma using the ISIS double-spectrograph, as service observations in 1994 July 23, kindly carried out for us by Dr V. Dhillon. The spectrograph provided two spectra in a single integration, one in the blue-wavelength region and another in the red. A 1200 line mm^{-1} grating was used, together with a Tektronix charge-coupled device (CCD) (1024 × 1024 pixels, 24-μm pixel size) on the blue arm, providing wavelength coverage from 5188 to 5593 Å, at a resolution of 0.84 Å FWHM. Each pixel along the slit projected to 0.358 arcsec on the sky. On the red arm, a 62 Å mm^{-1} grating was used with an EEV CCD (1248 × 1158 pixels, 22.5 μm pixel size) to cover the 8249–9967 Å wavelength region at a resolution of 3.3-Å FWHM. Each pixel along the slit projected to 0.335 arcsec on the sky. A dichroic filter having its '50 per cent power cut-point' at 6800 Å was used to split the light into the blue and red arms. A slit width of 1.033 arcsec was used throughout the nebular observations. Wide slitwidth (6.045 arcsec) observations of the *HST* standard star BD + 28° 4211 (spectral type Op, $V = 10.51$; Walsh 1993) were used for flux calibration. The seeing was about 0.9 arcsec FWHM during the observations. Two exposures, each of 30 min, were obtained for both the Ring Nebula and NGC 7027. For the Ring Nebula, the slit was oriented in PA = 156°, along its minor axis (Curtis 1918) and through the central star. For NGC 7027, the slit was at PA = 60°, again along the minor axis, and through the radio continuum centre (Masson 1989).

The data were reduced using standard methods for long-slit spectra, using IRAF[1] running on a DEC-station at UCL. The spectra were bias-subtracted, flat-fielded and were wavelength-calibrated via exposures of a copper–neon lamp. The small geometric distortions of the CCD spectra were accurately corrected for by a two-dimensional wavelength calibration. The sky background was subtracted by fitting low-order polynomials column-by-column to scan lines outside nebular emission. As described in Paper I, although the far-red wavelength region is crowded by strong sky OH emission lines, accurate sky subtraction can be achieved. The three [C I] lines of interest here are not affected by any nearby sky OH emission lines. The atmosphere extinction was corrected for by using the theoretical extinction curve for La Palma Observatory (RGO/La Palma Technical Notes, No. 31). The small contribution from dust extinction (wavelength independent) was incorporated by comparing the theoretical V-band extinction with values measured nightly by the Carlsberg Automatic Meridian Circle at La Palma. The monochromatic response curve used to put the spectra on an absolute flux scale was derived from the observations of the standard BD + 28° 4211, following the same algorithm described in Paper I.

Since the observations were not designed for the purpose of accurate radial velocity measurement, only one Cu–Ne wavelength calibration exposure was made after the two nebular exposures, each of 30 min. Therefore, in order to derive accurate radial velocities, some corrections were required, to account for the effects of instrument shift between the nebular and calibration exposures. The magnitude of wavelength drift can be determined by comparing the observed wavelengths of the same line measured on spectra from the first and second integrations and assuming that the drift between the two nebular exposures is twice as much as the drift between the second nebular exposure and the calibration exposure. We define the system radial velocity of a given line as that derived after integrating the line along the slit. After correction for the wavelength drift, the mean system heliocentric radial velocity derived for the Ring Nebula from the [N I] $\lambda\lambda 5198$, 5200, He II $\lambda 5411$ and [Cl III] $\lambda\lambda 5517$, 5537 lines, observed on the blue arm, was -22 ± 2 km s^{-1}, in agreement with the value of -19.2 ± 0.7 km s^{-1} given by Schneider et al. (1983). No significant differences were found between the system velocities derived from these lines, which are of very different excitation, suggesting a high degree of symmetry in velocity and emissivity distributions in the Ring Nebula. Similarly, from H I Pa 11 at 8862.787 Å, Pa 12 at 8750.475 Å, Pa 13 at 8665.384 Å, [C I] $\lambda\lambda 8727$, 9824, 9850 (with rest wavelengths taken from Paper I) and [S III] $\lambda 9531$, all observed on the red arm, we found a corrected mean system heliocentric velocity of -18 ± 3 km s^{-1} for the Ring Nebula, again in reasonable agreement with the value given by Schneider et al. The error on this latter determination is slightly larger

[1] IRAF is distributed by National Astronomy Observatories, which is operated by the Association of Universities for Research in Astronomy, Inc., under contract to the National Science Foundation.

than that deduced from the blue-arm spectra, reflecting the lower spectral resolution of the red-arm spectra. In addition to the systematic drift of spectral lines along the dispersion direction between the individual integrations, there can also be a small drift along the slit due to, e.g., telescope tracking and atmospheric refraction at different air masses. The Ring Nebula has a bright central star, thus the amount of shift of spectral lines along the slit between the two integrations, as a function of wavelength, could be determined by comparing the positions of the central star measured on the two spectra. The relative shifts between the two integrations were found to be the same within the errors ($\lesssim$0.1 pixel) at different wavelengths. However, within each frame the position of the central star does show small systematic variations from one end of the detector to the other, more pronounced on the blue-arm spectra than on the red-arm spectra, indicating that atmospheric differential refraction is the major cause, even though the spectra were taken close to the prime meridian and near the zenith (the air masses of the two exposures for the Ring Nebula were 1.016 and 1.045, respectively). Once the relative shifts were derived, both in the direction of dispersion and along the slit, their effects were corrected for by rebinning the spectra in both dimensions. The rebinned blue- and red-arm spectra from the two integrations were then averaged. All the measurements presented below were based on these average spectra.

Line fluxes and wavelengths were measured by fitting the lines with Gaussian profiles. No discernible departure of the spectral line profiles from Gaussians was found. The lines of the [N I] and [Cl III] doublets, as well as the [C I] $\lambda\lambda$9824, 9850 lines, were fitted simultaneously by the sum of two Gaussians of the same width and with their line centres fixed at the value given by the difference of their rest wavelengths. Since each pixel of the blue-arm and red-arm spectra projected along the slit to, respectively, 0.358 and 0.335 arcsec on the sky, and the seeing was about 1 arcsec, each spectral line of interest was measured by summing over three consecutive scan lines and stepping along the slit with a step size of one scan line. Actual measurements were done automatically, by writing a procedure using the facilities provided in the image processing package MIDAS.[2] A measurement was made only if, after the nebular continuum had been subtracted out, the peak intensity at the expected wavelength of the line of concern was three times larger than the standard deviation of the local continuum.

3 RESULTS AND DISCUSSION

3.1 Integrated line fluxes for NGC 6720 and 7027

The observed fluxes, $F(\lambda)$, of lines discussed in this paper, measured after integrating along the slit, are given in Table 1 for the Ring Nebula and NGC 7027. The fluxes $I(\lambda)$, corrected for interstellar reddening, are given by $I(\lambda)=F(\lambda)\times 10^{c(\mathrm{H}\beta)[1+f(\lambda)]}$, where $c(\mathrm{H}\beta)$ is the logarithmic extinction at Hβ and $f(\lambda)$ is the Galactic extinction curve from Howarth (1983). We adopt $c(\mathrm{H}\beta)=0.28$ for the Ring Nebula (Barker 1987) and $c(\mathrm{H}\beta)=1.37$ for NGC 7027 (Middlemass 1990).

[2]MIDAS is developed and distributed by the European Southern Observatory.

As described in Paper I, depending on the apparent radial velocity, the [S III] λ9531 and [C I] $\lambda\lambda$9824, 9850 lines can be affected by telluric absorption. Following the procedures described in Paper I, it was found that for the Ring Nebula the three lines are clear of telluric absorption. From the intensities listed in Table 1, we have $I(\lambda9850)/I(\lambda9824)=3.05$, in agreement within 3 per cent with the theoretical value of 2.96 derived from the transition probabilities of Nussbaumer & Rusca (1979). For NGC 7027, the λ9850 line is clear of telluric absorption, but not the λ9531 and λ9824 lines. For this object, we have $I(\lambda9850)/I(\lambda9824)=3.39$, which is 15 per cent larger than the theoretical value.

The diagnostic ratios $\Re_1\equiv I(\lambda9824+\lambda9850)/I(\lambda8727)$, $\Re_2\equiv I(\lambda5198)/I(\lambda5200)$ and $\Re_3\equiv I(\lambda5517)/I(\lambda5537)$, derived from the reddening-corrected intensities, are given at the end of Table 1. The intensity of the λ9824 lines has not been used in deriving $\Re_1$, instead we assumed $I(\lambda9824)=0.338\times I(\lambda9850)$, as given by their theoretical values. The ratio $\Re_1=27.7$ derived for the Ring Nebula is consistent with the lower limit of 14 estimated by Jewitt et al. (1983), who failed to detect the λ8727 line. The ratio is similar to those found for NGC 2346, 3132 and IC 4406 discussed in Paper I. It is much larger than the ratios predicted by radiative recombination of C^+ ions with electrons (Paper I) and is consistent with the collisional excitation of C^0 ions by electron impacts as the excitation mechanism. The observed ratio can thus be used to derive the electron temperature in the regions where the [C I] lines are emitted. However, the actual value of the [C I] line ratio depends on electron density as well, owing to the relatively low critical density of the nebular lines (cf. fig. 2 in Paper I). Since both

Table 1. Integrated line fluxes and diagnostic line ratios.

Line	NGC 6720		NGC 7027	
	$F(\lambda)$	$I(\lambda)$	$F(\lambda)$	$I(\lambda)$
	(10^{-13} erg cm^{-2} s^{-1})			
[N I] λ5198	0.758	1.37	4.00	72.3
[N I] λ5200	0.735	1.33	2.35	42.4
He II λ5411	0.621	1.08	77.5	1190
[Cl III] λ5517	0.257	0.443	3.41	49.2
[Cl III] λ5537	0.203	0.349	11.6	166.
H I λ8665 (Pa 13)	0.129	0.172	29.7	122.
[C I] λ8727	0.0591	0.0786	8.06	32.5
H I λ8750 (Pa 12)	0.157	0.208	35.6	143.
H I λ8863 (Pa 11)	0.215	0.284	51.5	201.
[S III] λ9531	8.52	10.9	942.	3150
[C I] λ9824	0.423	0.535	10.4	32.7
[C I] λ9850	1.29	1.63	35.6	111.
$\Re_1^a$		27.7		4.57
$T_e(\Re_1)$ (K)		8250		8100
$\Re_2^b$		1.03		1.71
$N_e(\Re_2)$ (cm^{-3})		650.		7640
$\Re_3^c$		1.27		0.296
$N_e(\Re_3)$ (cm^{-3})		560.		48000

[a]$\Re_1\equiv I(\lambda9824+\lambda9850)/I(\lambda8727)$. In calculating $\Re_1$, the flux of λ9824 was not used. Instead we assumed $I(\lambda9824)=0.338\times I(\lambda9850)$ (Nussbaumer & Rusca 1979).
[b]$\Re_2\equiv I(\lambda5198)/I(\lambda5200)$.
[c]$\Re_3\equiv I(\lambda5517)/I(\lambda5537)$.

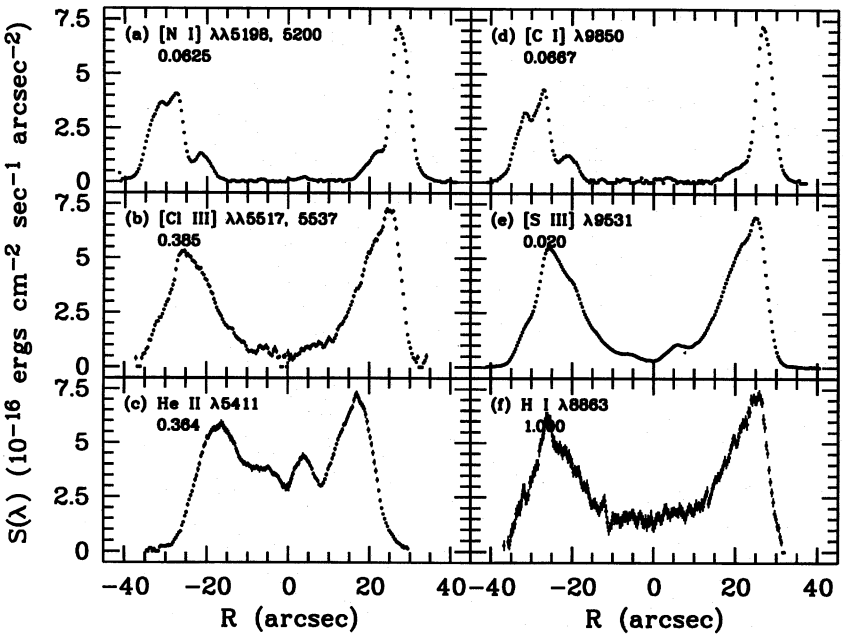

Figure 1. The observed surface brightness distributions of some selected lines along the minor axis of the Ring Nebula. The surface brightness distribution plotted in each panel has been scaled by multiplying by the number given under the identification. No correction for interstellar reddening has been made. Positive R corresponds to the north-western side of the minor axis.

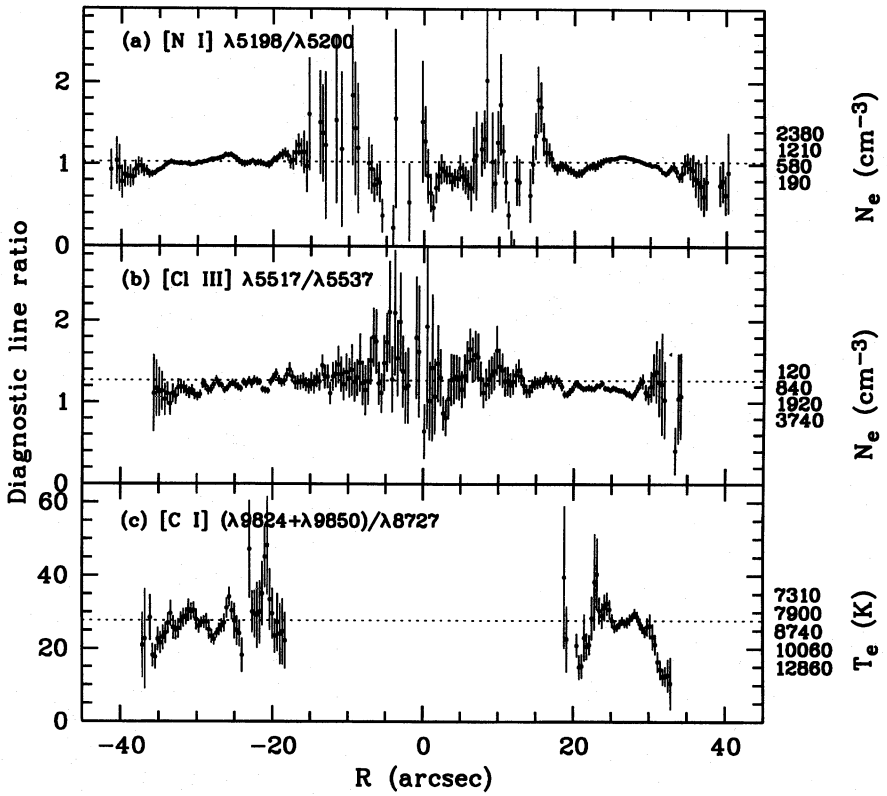

Figure 2. The (a) [N I], and (b) [Cl III] doublet ratios and (c) the reddening-corrected [C I] (λ9824 + λ9850)/λ8727 ratio, along the minor axis of the Ring Nebula. The dashed line in each panel shows the average ratio derived after integrating the lines along the slit. In (a) and (b) electron densities corresponding to the [N I] and [Cl III] doublet ratios are given to the right of the plots. For the [N I] doublet, these densities are for an electron temperature of $T_e = 8250$ K, the mean temperature deduced from the integrated [C I] line ratio. For the [Cl III] doublet, a temperature of $T_e = 10\,000$ K is assumed (Barker 1987). In (c) the electron temperatures T_e implied by the [C I] line ratios by the tick marks are shown to the right of the plot, assuming a mean electron density of $N_e = 650$ cm^{-3}, as derived from the integrated [N I] doublet ratio. See also the caption to Fig. 1, as well as the text, for more details.

the surface brightness and radial velocity of the [C I] and [N I] lines (Sections 3.2 and 3.3, Figs 1 and 3) show nearly identical distributions along the nebular minor axis, we assumed that the [C I] and [N I] lines originate from the same regions in the nebula and we determined the electron temperature and density in these regions by fitting the observed [C I] nebular to auroral line ratio, and the [N I] doublet ratio, simultaneously. We find $T_e(\Re_1)=8250$ K and $N_e(\Re_2)=650$ cm^{-3}. The atomic parameters used were the same as in Paper I except for the fine structure levels of the ground term of C^0, $2p^2\,^3P_{0,1,2}$, for which the effective collision strength were updated to those of Johnson, Burke & Kingston (1987). The update does not affect the results for $T_e(\Re_1)$, but will affect the discussion of the [C I] fine structure line at 609 μm given below. The [Cl III] density of $N_e(\Re_3)=560$ cm^{-3} for the Ring Nebula was derived assuming an electron temperature of 10 000 K (Barker 1987). It is slightly smaller than that from the [N I] lines, but the difference may not be significant.

The small ratio of $\Re_1=4.57$ derived here for the [C I] lines from NGC 7027 confirms the early results of Danziger & Goad (1973), who estimated $\Re_1=3.44$ (they used a reddening constant of $c(\mathrm{H}\beta)=1.40$, which is only slightly larger than the value of 1.37 adopted here).[3] They pointed out that collisional de-excitation of the upper level of the [C I] nebular lines, ^{1}D, which has a relatively small critical density ($\sim 1.6\times10^4$ cm^{-3} at $T_e=10\,000$ K; Paper I), is responsible for the small value of $\Re_1$ observed in NGC 7027. A recent analysis of a number of temperature and density diagnostics for NGC 7027 was given by Middlemass (1990). Remarkably, a very good convergence is achieved at $T_e=13\,500$ K and $N_e=50\,000$ cm^{-3}. For the two density diagnostic ratios $\Re_2$ and $\Re_3$ measured here, we have $N_e(\Re_2)=7640$ cm^{-3} and $N_e(\Re_3)=48\,000$ cm^{-3}. The small value of N_e derived from $\Re_2$ can be attributed to the relatively small critical densities of the [N I] lines, about 4880 and 1750 cm^{-3} at $T_e=10\,000$ K for the upper levels of the λ5198 and λ5200 lines, respectively. Indeed, the observed value of $\Re_2=1.71$ is within 8 per cent of 1.85, the limit at infinite density. In contrast, the [Cl III] doublet has much higher critical densities, about 2.4×10^4 and 1.6×10^5 cm^{-3} at $T_e=10\,000$ K for the upper levels of the λ5517 and λ5537 lines, respectively. The density derived from the [Cl III] lines, $N_e(\Re_3)=48\,000$ cm^{-3}, is in excellent agreement with the results of Middlemass (1990). Thus, it is likely that the [N I] doublet ratio measured here has substantially underestimated the real electron density in its region of emission around NGC 7027. Middlemass's analysis of the Mg I] λ4562/λ4571 ratio, which is likely to be emitted in the same regions as the [C I] and [N I] lines, gives $N_e(\Re_3)=49\,000$ cm^{-3}, in close agreement with the densities derived from the [Cl III] doublet and other density diagnostics. If we assume that $N_e=48\,000$ cm^{-3}, as derived from the [Cl III] and Mg I] doublets, is also representative of the [C I] emitting regions, then the measured [C I] ratio $\Re_1$ yields an electron temperature of $T_e(\Re_1)=8100$ K, significantly lower than the 13 500 K deduced for the ionized regions (Middlemass 1990).

The mean [C I] temperature derived for the Ring Nebula is about 1800, 1450 and 1120 K lower, respectively, than the average temperatures derived by Barker (1987) from the [O III] and [N II] lines and from the nebular Balmer discontinuity, for several regions in the Ring Nebula. The result is similar to what we found in Paper I for three other nebulae, i.e. NGC 2346, 3132 and IC 4406, where the mean [C I] temperature was about 1800–2800 K lower than those derived from the higher excitation [N II], [S III] and [O III] lines, suggesting a general decrease of electron temperature from the ionized regions into the transition regions to the neutral zones. Whereas such a general decrease in temperature is predicted by nebular photoionization modelling calculations (e.g. fig. 5a in Liu et al. 1995b), no calculations of this type include molecular processes. On the other hand, in modelling calculations of the thermal structure and chemistry of PDRs (e.g. Escalante et al. 1991) the radiative fields are imposed as a free parameter. Quantitative interpretation of the results presented here requires modelling calculations including both radiative atomic and molecular processes, as well as a consistent treatment of the thermal and ionization structure and of the radiative transfer from the ionized, central part of the nebula into the transition regions and the neutral zones.

3.2 Surface brightness distributions for NGC 6720

The large spatial extension of the Ring Nebula and the deep spectra obtained here allow us to map the relatively weak [C I] and [N I] lines in this nebula. Studies of the surface brightness distribution in the Ring Nebula can be traced back to as early as Curtis (1918). By comparing the peak surface brightness in the bright ring with that at the nebular centre, Curtis showed that the Ring Nebula cannot be a homogeneous closed shell of gas. Extending his work, Minkowski & Osterbrock (1960) postulated a toroidal model for the nebula. Monochromatic images in a number of lines and more recent structural studies of the Ring Nebula are presented by Louise (1974), Reay & Worswick (1977), Kupferman (1983), Chu, Jacoby & Arendt (1987), Balick (1987) and Balick et al. (1992).

The observed surface brightness distributions along the minor axis of the Ring Nebula for some selected lines are presented in Fig. 1. The distributions of the [N I] doublet and of the [C I] λ9850 line are nearly identical to each other. So too are the [Cl III] and [S III] distributions. The four lines all have very low surface brightness near the nebular centre, where the relevant elements are ionized to higher ionization stages. For H I Pa 11 at λ8863, the ratios of the peak surface brightness in the ring to that at the nebular centre fall between 4.3 and 5.0, consistent with previous determinations (e.g. Kupferman 1983). As first shown by Curtis (1918), the large peak to central brightness ratio, together

[3]In their low-resolution sequential scanner observations (exit slit 80 Å), the λ8727 line was blended with Pa 12. From the observed fluxes of Pa 7, Pa 9 and Pa 10 and assuming that the relative intensities of the Paschen lines were given by radiative recombination theory, Danziger & Goad found the flux of Pa 12 to be about 1.23 times higher than expected and ascribed all of this excess to the [C I] λ8727 line. Although their high-resolution photographic image tube spectroscopy of this wavelength region found no extra lines other than λ8727 within 60 Å of Pa 12, our deeper observations reveal weak emission lines from He II λ8701.7, He I λ8733.8, He I λ8776.8 and an unidentified feature at 8706.9 Å (see also Péquignot & Baluteau 1988). The total flux of these weak lines amounts to 50 per cent of the λ8727 line. This may explain the slightly lower value of $\Re_1$ found by them.

with the large thickness of the shell, indicate that the H I-emitting regions in the Ring Nebula cannot be closed, spherically symmetric shells. Similar statements can be made for the [Cl III]- and [S III]-emitting regions, from the data shown in Fig. 1. In contrast to other lines, the He II λ5411 line has a much smaller peak to central brightness ratio. Part of the difference can be attributed to the general decrease of ionization degree from the centre to the outer parts of the nebula, where most of the He^{2+} ions recombine to He^{+}. However, Reay & Worswick (1977) and Kupferman (1983) argue that unlike the bright ring, the central He II emission region of the Ring Nebula is more likely to be a closed shell. Compared with lines from ionized species, the surface brightness distributions of the [C I] and [N I] doublets show a much more complicated structure. The north-western part of the minor axis is characterized by a very sharp narrow peak near radius $R \sim +27$ arcsec, just outside the peak brightness of H I Pa 11. Within this is a weak broad component starting from $R \sim +17$ arcsec. On the other side of the minor axis, three components can be identified. Note there is some weak emission near $R \sim +4$ arcsec and $R \sim -7$ arcsec, seen both in the [C I] and [N I] lines. These two very weak components have very large and opposite radial velocities (Fig. 3) relative to the system velocity (Section 3.3), indicating that they come from material in the front and rear parts of the nebula, respectively, far from the nebular centre. Further discussion of the surface brightness distributions shown in Fig. 1 is given in Section 3.3, in connection with the results from radial velocity measurements.

Variations of the [N I], [Cl III] and [C I] diagnostic line ratios, $\Re_2$, $\Re_3$ and $\Re_1$ along the minor axis of the Ring Nebula, are plotted in Fig. 2. Mapping the [C I] line ratios along the slit involves comparing the surface brightnesses of two lines of significantly different wavelengths, thus complications arise due to the effects of atmospheric differential refraction, where spectral lines of different wavelengths drift slightly along the slit systematically as a function of wavelength. As a result, two pixels of the same scan line at different wavelengths sample slightly different regions of the nebula, yielding systematic errors in the line ratio if the intensities measured at the two pixels are simply divided without any correction. The apparent drifts of spectral lines along the slit as a function of wavelength could be determined by measuring the position of the central star at different wavelengths. For the spectra of the Ring Nebula

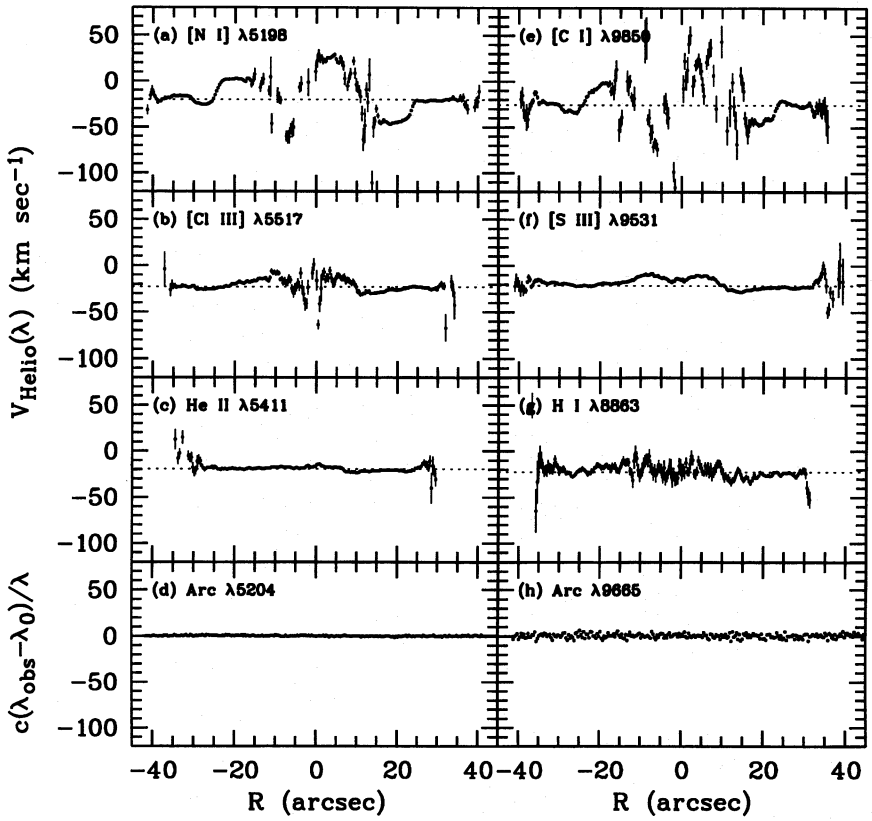

Figure 3. Heliocentric radial velocities of six nebular lines along the minor axis of the Ring Nebula. The three nebular lines plotted in the three top left panels are derived from the blue-arm spectra which have a spectral resolution of 0.84-Å FWHM. The three lines shown in the right panels were deduced from red-arm spectra with a resolution of 3.3 Å. The dashed line in each of the six panels indicates the system velocity of each line as derived after integrating the line flux along the slit. The bottom two panels show the wavelength calibration residuals in terms of velocity, $c\Delta\lambda/\lambda_0 \equiv c\,(\lambda_{obs} - \lambda_0)/\lambda_0$, where λ_{obs} and λ_0 are, respectively, the observed and laboratory wavelengths and c is the velocity of light, for two copper–neon calibration lines, λ5203.895 and λ9665.424. The arc line λ5204 is close in wavelength to the [N I] line shown in the top left panel, whereas the arc line λ9665 is the nearest calibration line to the [C I] line plotted in the top right panel. There are no usable calibration lines beyond λ9665 from the copper–neon arc spectra. In the bottom two panels the error bars are too small to be seen on this scale. See also the caption of Fig. 1.

discussed here, the drift was found to be 0.76 pixel, or 0.254 arcsec projected on to the sky, between 8727 and 9850 Å. Although the amount of drift may seem small, it can introduce significant errors in the line ratios if it is not corrected for, because of the very steep variations in the surface brightness distributions of the [C I] lines along the nebular minor axis (for the λ9850 line, $\Delta S/S \sim 0.25$ pixel^{-1} at $R = 25$ arcsec; cf. Fig. 1). The drifts of the sampling region perpendicular to the slit cannot be determined from the current data. However, since the slit is oriented along the minor axis and the bright ring in the Ring Nebula is relatively smooth perpendicular to its minor axis, only relatively small errors are expected due to any possible small drift of the sampling region in this direction as a function of wavelength and its possible effects are therefore neglected in our analysis. To correct for the effects of the drift along the slit, we rebinned the surface brightness distribution of the λ8727 line such that it could be compared directly to that of the λ9850 line. For the [N I] and [Cl III] doublet ratios, the effects of atmospheric differential refraction are negligible, owing to the small wavelength difference of the lines involved. Finally, as described in Section 3.1, for the apparent mean radial velocity of the Ring Nebula during the observations, both the [C I] nebular lines at $\lambda\lambda$9824, 9850 would have been clear of telluric absorption. Since the λ9850 line is three times stronger than the λ9824 line, only the intensity of the former line was used to calculate the ratio $\Re_1$. The same practice was followed in deducing the ratios $\Re_1$ plotted in Fig 2. For pixels with a measured λ9850 line surface brightness larger than 1.5×10^{-16} erg cm^{-2} s^{-1} arcsec^{-2} (163 points in total), the derived mean $I(\lambda 9850)/I(\lambda 9824)$ ratio is 2.94 ± 0.49, for all points equally weighted, which is in excellent agreement with the theoretical value of 2.96. As seen in Fig. 3, the radial velocity of the [C I] emission shows dramatic variations along the minor axis of the Ring Nebula. There are two atmospheric water vapour absorption lines of significant strength at 9849.12 and 9848.90 Å. Following the procedures described in Paper I, it is found that the [C I] λ9850 line may be affected by these two water vapour lines if the heliocentric radial velocity $V_\odot \lesssim -40$ km s^{-1}. Figs 3(a) and (e) in Section 3.3 show that this may apply to a few points near $R \sim +20$ arcsec whose ratios are plotted in Fig. 2(c). We see in Fig. 2(c) that the points between $+19 \lesssim R \lesssim +22$ arcsec do indeed have values of $\Re_1$ which are systematically lower than the mean value. On the other hand, for these same points we find $\lambda 9850/\lambda 9824 = 3.00 \pm 0.29$, where the error corresponds to one sigma standard deviation, consistent with the theoretical value of 2.96. Since the λ8727 and λ9824 lines are clear of telluric absorption, this result suggests that the small values of $\Re_1$ found for the points near $R \sim +20$ arcsec are probably not due to telluric absorption of the λ9850 lines and thus could be caused by higher temperatures.

The electron densities implied by the [N I] and [Cl III] doublet ratios in Figs 2(a) and (b), and the electron temperatures given by the [C I] nebular to auroral line ratio in Fig. 2(c), are shown to the right of the plots. As before, for the [N I] doublet ratio the derived densities are for an electron temperature of $T_e = 8250$ K, the electron temperature derived from the integrated [C I] line ratio. For the [Cl III] lines, $T_e = 10\,000$ K was assumed (Barker 1987). The electron temperatures given by the tickmarks at the right of Fig. 2(c) were calculated for a constant electron density of $N_e = 650$ cm^{-3}, the density derived from the integrated [N I] doublet ratio. Figs 2(a) and (b) show that the electron density remains fairly constant across the minor axis of the Ring Nebula. There are, however, some discernible variations. The bright ring seems to have a slightly higher density, approaching 1000 cm^{-3}. Although the data are quite noisy inside the bright ring, the central part of the nebula seems to have lower densities. For a spectrum integrated over $|R| < 15$ arcsec, line profile fitting to the [Cl III] $\lambda\lambda$5517, 5537 lines gives $\lambda 5517/\lambda 5537 = 1.35 \pm 0.05$, yielding $N_e = 270^{+180}_{-150}$ cm^{-3}. For the [N I] lines similar measurements are more difficult, due to the weakness of the lines. We notice that near $R \sim -7$ and $+4$ arcsec, where the [N I] lines are better measured, Fig. 2(a) shows a clearly lower [N I] density, about 200 cm^{-3}. As noted above, the [N I] emission at these two positions is likely from material in the front and rear parts of the nebula, far from the nebular centre. The low densities derived from the [Cl III] doublet ratio for the central region of the Ring Nebula are consistent with the maximum density of 290 cm^{-3} derived by Kupferman (1983) for the same region from the He II volume emissivity. There is an [N I] high-density spike in Fig. 2(a) near $R \sim +16$ arcsec. No similar [Cl III] high-density spike is found in Fig. 2(b). It is not clear whether the [N I] density spike is caused by some low-ionization high-density clumps or simply by some unknown errors. Outside the bright ring ($|R| \gtrsim 30$ arcsec), the [N I] electron density shows a clear general decrease, probably as a result of most of the gas having become neutral beyond this radius.

Fig. 2(c) shows some discernible variations in the [C I] ratio $\Re_1$ along the nebular minor axis. In the bright ring itself, the ratio gives an electron temperature around 8200 K. Outside the ring, the ratio decreases systematically, suggesting higher electron temperatures. As described earlier, the small ratios found near $R \sim +20$ arcsec may also be real. The emission near this position comes from a broad component at the inner part of the bright ring (Fig. 1d). Within the south-eastern ring there are also some variations in $\Re_1$ along the minor axis. The local maximum and minimum of $\Re_1$ at $R \sim -31$ and -27 arcsec correspond to the two local maxima seen in the [C I] line surface brightness (Fig. 1d). Thus, it seems that there are some real temperature variations, at the level of $\lesssim 2000$ K, among the different [C I]- and [N I]-emitting regions in Figs 1(a) and (d). As we will see in Section 3.3, these different regions have quite distinct radial velocities, and thus are likely to correspond to different parts of the nebula. Although the higher electron temperature found from the [C I] lines near $R \sim +20$ arcsec can be attributed to higher electron temperatures in the nebular central regions (e.g. Kupferman 1983), the increase in the [C I] temperature outside the bright ring is more difficult to understand. Deep CCD imaging of the Ring Nebula (Chu et al. 1987; Balick et al. 1992) reveals two limb-brightened Hα + [N II] haloes far beyond the bright ring, indicating the presence of residual ionization in the neutral zone. This could support a scenario for the Ring Nebula whereby the rapidly declining luminosity of the central star, on the white dwarf cooling track, has led to the retreat of the ionization front and the recombination of previously ionized material (Barlow, Rawlings & Drew, in preparation). If this is the case, then the observed decrease of the [C I] ratio

$\Re_1$ outside the bright ring might be interpreted as due to contamination of the [C I] lines by contributions from the recombination of C^+ ions with electrons. As we show in Paper I, recombination of C^+ ions with electrons produces much smaller ratios of $\Re_1$, $\lesssim 10$, with the ratios not being indicative of the actual temperature.

Recently, Bachiller et al. (1994) have reported the detection of the [C I] 609 μm fine-structure line in the Ring Nebula, the first detection of this line in a planetary nebula. They mapped this line with a beam size of 15 arcsec, as well as the CO $J=2-1$ line with a beam size of 12 arcsec, at a number of positions along the minor axis and found that both lines had a similar spatial distribution, with the peak emission occurring near the bright ring. It is likely that both lines come from the same regions as the H_2 near-infrared emission lines (Greenhouse et al. 1988; Kastner et al. 1994), close to the transition regions. It is thus interesting to compare our observations of the optical [C I] lines to Bachiller et al.'s submillimetre fine-structure line data. For this purpose we digitized their [C I] 609 μm line spectra (fig. 1 in their paper). The spectra are, however, quite noisy, and if we average the five spectra plotted by them, the signal is lost in the noise. However, the line is clearly detected and has the best signal-to-noise ratio at Position B in their paper (10 arcsec west and 20 arcsec south of the central star). For this position, fitting the double-peaked line profile with two Gaussians yields a line flux of 6.52 ± 1.00 K km s^{-1}, which is equivalent to a surface brightness of $(1.87 \pm 0.28) \times 10^{-17}$ erg cm^{-2} s^{-1} arcsec^{-2}. The average surface brightness of the [C I] λ9850 line between $-29.9 < R < -3.7$ arcsec (the range in R covered by their panel B spectrum) is found to be 1.49×10^{-15} erg cm^{-2} s^{-1} arcsec^{-2}, or 1.87×10^{-15} erg cm^{-2} s^{-1} arcsec^{-2} after correcting for interstellar reddening using $c(\mathrm{H}\beta)=0.28$. Thus, we have $\Re_4 \equiv \lambda 9850/609\ \mu\mathrm{m} = 100$. For the case where both lines originate from the same temperature region, the kinetic temperature of the region implied by this line ratio is between 1500 and 3100 K, provided the density is higher than 100 cm^{-3}. An error of a factor of 2 in the ratio $\Re_4$ would increase the derived temperature range only slightly, to 1400–3600 K. This temperature range is, however, much lower compared with the mean value of 8250 K deduced from the nebular to auroral line ratio and indicates that most of the 609-μm line flux originates from cooler, presumably mainly neutral regions, with the line being excited by collisions with atomic and molecular hydrogen. For $T_e = 8250$ K and $N_e = 650$ cm^{-3}, the mean electron temperature and density derived from the optical [C I] and [N I] lines in Section 3.1, we have $I(\lambda 9850)/I(609\ \mu\mathrm{m}) = 1.9 \times 10^4$, which is 190 times higher than the observed ratio of 100. Thus, the warm transition regions around the Ring Nebula contribute less than 1 per cent of the total flux of the 609 μm line observed from this nebula.

3.3 The radial velocities measured for NGC 6720

The variations of the heliocentric radial velocities of a number of emission lines along the minor axis of the Ring

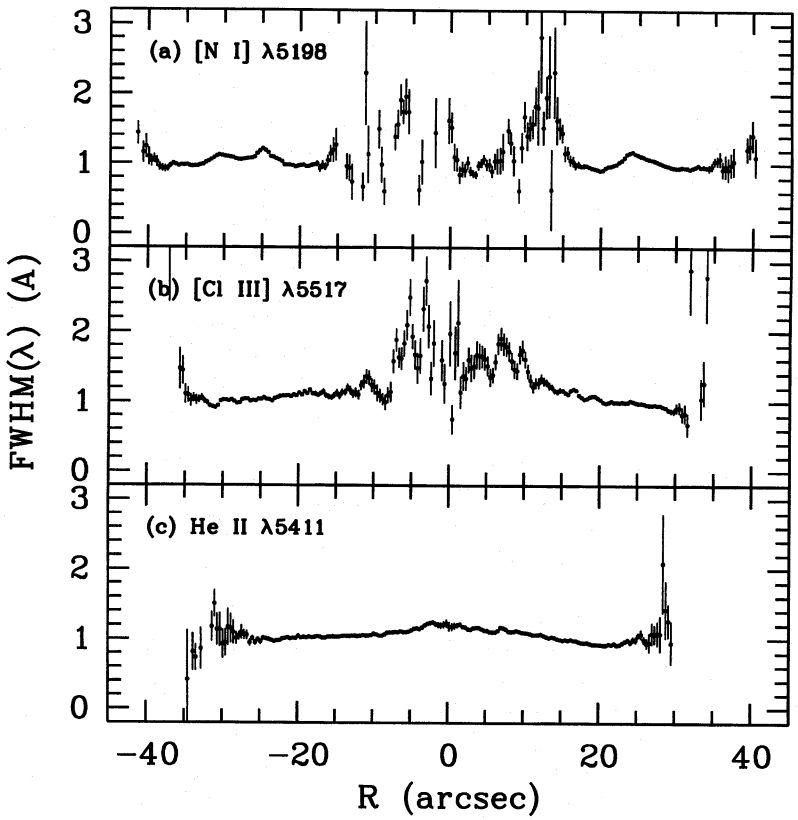

Figure 4. FWHMs of the [N I] λ5198, [Cl III] λ5517 and He II λ5411 lines along the minor axis of the Ring Nebula. The linewidths are dominated by instrumental broadening, which, however, does not vary along the slit. See also the caption of Fig. 1.

Nebula are shown in Fig. 3, while their FWHMs are shown in Fig. 4. The system velocity of each line, defined as the velocity derived after integrating the line along the slit, is indicated in Fig. 3 as a dashed line. The three nebular lines shown on the three top left panels of Fig. 3 were observed on the blue arm with a spectral resolution of 0.84-Å FWHM, whereas the three nebular lines on the right were observed on the red arm with a resolution of 3.3 Å. The most remarkable feature in Fig. 3 is the dramatic yet nearly identical variations in the [C I] and [N I] radial velocities. The variations are nearly absent in the lines from ionized species. Some small velocity variations can be seen in the [Cl III] and [S III] lines, with a magnitude of 15 km s^{-1}, but the variations are limited to regions inside the bright ring ($|R| \lesssim 10$ arcsec). To show that the observed variations are not due to flawed calibration, the residuals, in terms of velocity, of two calibration arc lines, one close in wavelength to the [N I] lines and the other close to the [C I] lines, are shown in the bottom two panels of Fig. 3. Another remarkable feature of Fig. 3 is the nearly perfect point symmetry in the [C I] and [N I] radial velocity distributions with respect to the nebular centre. In Figs 3(a) and (e), seven components with very different velocities can be identified, i.e. (i) $R \gtrsim +25$ arcsec; (ii) $+15 \lesssim R \lesssim +24$ arcsec; (iii) near $R \sim +4$ arcsec; (iv) near $R \sim -7$ arcsec; (v) $-23 \lesssim R \lesssim -17$ arcsec; (vi) $-30 \lesssim R \lesssim -25$ arcsec; and (vii) $R \lesssim -31$ arcsec. Remarkably, the positions of these seven components correspond nicely with the seven [C I] and [N I] emission maxima identifiable in Figs 1(a) and (d). Between each of these components, the radial velocity changes abruptly by large amounts, sometimes from blue-shifted to redshifted, relative to the system velocity, by as much as 70 km s^{-1} (e.g. between (ii) and (iii)). This happens even on the same side of the nebula more than once. Both the radial velocity and surface brightness distributions of the [C I] and [N I] lines along the minor axis of the Ring Nebula strongly support the bipolar end-on model proposed for this nebula by Bryce et al. (1994, fig. 11) and suggest that the neutral [C I] and [N I] lines form in the equatorial torus as well as within the walls of the two lobes blown up by the fast wind. In this picture, the dramatic variations of velocity between $-25 \lesssim R \lesssim +25$ arcsec can be interpreted as due to the change in the relative contributions to the observed line fluxes from the front and rear lobes, as the line-of-sight moves from one end to the other. The emission from velocity region (i) and from regions (vi) and (vii), listed above, is obviously mainly from the dense equatorial torus. Note that at $R = 0$ arcsec, the [N I] and [C I] have a redshifted radial velocity of $\sim +35$ km s^{-1} relative to the system velocity. This is not unexpected in the model of Bryce et al. (1994), where the line-of-sight has a finite inclination angle with respect to the nebular symmetry axis.

The emission regions (ii) and (v) are clearly from the walls of the two lobes in the very vicinity of the bright ring. The finite inclination angle, the faintness of emission from the lobes as compared with that from the ring (see Fig. 1a), as well as the relatively low spectral resolution, together explain why at the north-western part of the minor axis (positive radius R), we see only emission from the blue-shifted, front lobe (emission region ii) which projects on the sky inside the ring, but not the emission from the rear, redshifted lobe, which projects on the sky overlapping with the bright ring. Similarly, on the other side of the minor axis, we see only emission from the rear, redshifted lobe (emission region v), projected on the sky inside the ring. The high outflow velocities of the transition zone material along the walls of the two lobes in the vicinity of the bright ring can be inferred from the velocity jumps between velocity regions (i) and (ii), ~ -25 km s^{-1}, and between regions (vi) and (vii) and (v), $\sim +23$ km s^{-1}. The near equivalence in absolute magnitude of the two velocity jumps suggest that in the very vicinity of the ring, the two lobes are nearly normal to the equatorial plane, i.e. parallel to the polar axis. For an inclination angle of 45° (Minkowski & Osterbrock 1960), the linear velocity of material within the walls relative to the ring is thus $\sim 24 \times \cos^{-1} 45° = 34$ km s^{-1}. Such a high outflow velocity might be due to the high ram pressure generated at the inner part of the confining torus by a fast stellar wind. High-velocity particles carried by the fast wind would hit the dense torus, and be reflected away nearly tangentially, dragging with them material entrained from the ring in a mass-loaded flow. It is very likely that strong shocks would be generated near the interfaces between the transition zones and the neutral envelope. Such shocks may provide a natural excitation mechanism for the strong near-infrared H_2 emission observed from the Ring Nebula (e.g. Kastner et al. 1994).

The FWHM distributions plotted in Fig. 4 for three lines measured on the blue-arm spectra, taken at a resolution of 0.84 Å, show some significant variations across the nebular minor axis. Even though the linewidths shown in this diagram are dominated by instrumental broadening, the latter does not of course change with slit position. As expected, the linewidths are largest in the central regions, and there is a general increase in linewidth on going from lines of higher ionization degree to lines of lower ionization degree, suggesting that the Ring Nebula has a differential expansion structure, with the velocity increasing with radius. The FWHMs of the [N I] lines show very complicated variations, with several distinct sharp peaks. Comparison between Figs 3 and 4 shows that these peaks occur at positions where the radial velocity changes abruptly, i.e. at the edges of the individual emission components seen in Figs 1(a) and (d) and Figs 3(a) and (e).

An interesting point can be drawn from the flatness of the H I Pa 11 λ8863 radial velocity distribution shown in Fig. 3(g). The peak surface brightness of Pa 11 occurs at $R = \pm 25$ arcsec along the minor axis (Fig. 1f). Thus, at these two positions the Pa 11 line emission should be dominated by the bright ring. However, Fig. 3(g) shows that the difference in radial velocity between these two positions is essentially zero within the errors. Quantitatively, we have $\Delta V_{\rm hel} = 1 \pm 3$ km s^{-1}. For the inclination angle of 45° inferred for the bright ring (Minkowski & Osterbrock 1960), this yields a very low expansion velocity, less than $4 \times \cos^{-1} 45° = 5.6$ km s^{-1}.

4 SUMMARY

For the first time, the [C I] λ8727 line has been detected in the Ring Nebula and the [C I] lines mapped along the minor axis. The [C I] nebular to auroral line ratio (λ9824 + λ9850)/λ8727 yields a mean electron temperature

of 8250 K for the warm transition regions around the Ring Nebula. Temperature variations of up to 2000 K are observed from different parts of the nebula. From the density-sensitive [N I] doublet ratio, $\lambda5198/\lambda5200$, we find an electron density in the transition regions which is similar to those inferred for the ionized regions. Compared with lines from ionized species, the [C I] and [N I] lines show dramatic and complicated varations, in both their surface brightness distributions and their radial velocities across the nebular minor axis. The variations are consistent with the end-on bipolar model proposed by Bryce et al. (1994) for the Ring Nebula, with these neutral lines formed in the optically thick equatorial torus, as well as within the walls of the two lobes blown up by the fast winds.

The large outflow velocities in the transition regions (up to ± 35 km s^{-1}) compared with those in the ionized regions revealed by our spectra suggest that strong shocks should be generated by these bulk material movements. These shocks would provide a natural excitation mechanism for the strong near-infrared molecular H_2 emission lines observed from the Ring Nebula (e.g. Kastner et al. 1994). Further observations of these neutral atomic transitions, including those from [O I], using higher spatial and spectral resolution, may prove to be very fruitful in interpreting the excitation of the near-infrared and millimetre-wave molecular lines observed from the Ring Nebula.

We have also measured the [C I] and [N I] lines in NGC 7027. The results confirm the small value of the [C I] $(\lambda9824+\lambda9850)/\lambda8727$ ratio found by Danziger & Goad (1973), caused by collisional de-excitation at the high densities characteristic of NGC 7027.

ACKNOWLEDGMENTS

We thank Dr V. Dhillon for kindly carrying out the WHT service observations presented here. We are grateful to Dr M. Bryce for a critical reading of the original manuscript. Useful comments from Drs J. Meaburn and G. Mellema are also acknowledged here.

REFERENCES

Bachiller R., Huggins P. J., Cox P., Forveille T., 1994, A&A, 281, L93
Balick B., 1987, AJ, 94, 671
Balick B., Gonzalez G., Frank A., Jacoby G., 1992, ApJ, 392, 582
Barker T., 1987, ApJ, 322, 922
Bryce M., Balick B., Meaburn J., 1994, MNRAS, 266, 721
Chu Y. H., Jacoby G. H., Arendt R., 1987, ApJS, 64, 529
Cox P., Omont A., Huggins P. J., Bachiller R., Forveille T., 1992, A&A, 266, 420
Curtis H. D., 1918, Publ. Lick Obs., 13, 57
Danziger I. J., Goad L. E., 1973, Astrophys. Lett., 14, 115
Escalante V., Sternberg A., Dalgarno A., 1991, ApJ, 375, 630
Greenhouse M. A., Hayward T. L., Thronson Jr, H. A., 1988, ApJ, 325, 624
Howarth I. D., 1983, MNRAS, 203, 301
Jewitt D. C., Kupferman P. N., Danielson G. E., Maran S. P., 1983, ApJ, 268, 683
Johnson C. T., Burke P. G., Kingston A. E., 1987, J. Phys. B., 20, 2553
Kastner J. H., Gatley I., Merrill K. M., Probst R., Weintraub D. A, 1994, ApJ, 421, 600
Kupferman P. N., 1983, ApJ, 266, 689
Liu X.-W., Barlow M. J., Danziger I. J., Clegg R. E. S., 1995a, MNRAS, 273, 47 (Paper I)
Liu X.-W., Barlow M. J., Blades J. C., Osmer S., Clegg R. E. S., 1995b, MNRAS, 276, 167
Louise R., 1974, A&A, 30, 189
Masson C. R., 1989, ApJ, 336, 294
Middlemass D., 1990, MNRAS, 244, 294
Minkowski R., Osterbrock D. E., 1960, ApJ, 131, 537
Münch G., Hippelein H., 1982, Ann. NY Acad. Sci., 395, 170
Nussbaumer H., Rusca C., 1979, A&A, 72, 129
Péquignot D., Baluteau J.-P., 1988, A&A, 206, 298
Reay N. K., Worswick S. P., 1977, MNRAS, 179, 317
Reay N. K., Walton N. A., Atherton P. D., 1988, MNRAS, 232, 615
Richer M. G., McCall M. L., Martin P. G., 1991, ApJ, 377, 210
Schneider S. E., Terzian Y., Purgathofer A., Perinotto M., 1983, ApJS, 52, 399
Storey J. W. V., 1984, MNRAS, 206, 521
Walsh J. R., 1993, ST-ECF Newsletter, 19, 6
Zuckerman B., Gatley I., 1988, ApJ, 324, 501